Atmospheric Phase Compensation in Extreme Weather Conditions for Ground-Based SAR

Amila Karunathilake, *Member, IEEE*, and Motoyuki Sato, *Fellow, IEEE*

***Abstract*—Herein, a semiempirical model is proposed to remove the atmospheric phase screen (APS) that occurs during ground-based synthetic aperture radar (GB-SAR) monitoring in steep mountainous areas with extreme weather conditions. The proposed method is based on a model-based statistical technique, which combines the topographical information and the estimated phase of interferograms. A 3-D geographical model was designed to investigate the effect of topographical irregularities, such as elevation, slope, and their correlation with the APS. The observed phases were then modeled according to the altitude and range of the 3-D topographical structure seen by the radar. A two-stage semiempirical algorithm is proposed to compensate for the APS in the spatial domain. Herein, the temporal changes in meteorological parameters, such as the atmospheric temperature, pressure, or humidity, were not considered for phase correction, drastically reducing the model background information and providing faster data processing for real-time GB-SAR monitoring. The proposed model was applied to the mountainous environment of a road reconstruction site in Minami-Aso, Kumamoto, Japan, where large-scale landslides were triggered after the Kumamoto earthquake in April 2016.**

***Index Terms*—Displacement measurement, interferometry, radar, remote sensing.**

I. Introduction

ENVIRONMENTAL changes caused by abrupt natural disasters affect the consistency of currently used statistical landslide estimation models. Model-based estimations using remotely sensed data can provide more facile and accurate information than those by conventional methods [1], [2], which is important for disaster-prevention and decision making. Unlike space-borne and airborne radar remote sensing techniques, ground-based synthetic aperture radar (GB-SAR) is ideal for monitoring the competence of small-scale areas in urban environments, such as buildings and bridges, other manmade structures [3], and for observing disaster-affected environments for landslides or other land deformations [4]. The high-sensor platform stability, narrow frequency bandwidth [5], and short revisit time of GB-SAR provide better spatial and temporal resolution, leading to more accurate quantitative measurements of ground movement, kinematic analysis, and understanding of the dynamics of unstable areas threatened by terrain movement [6]. Additionally, the use of the differential interferometric SAR (DInSAR) technique in GB-SAR offers the possibility of obtaining a 2-D map of the ground area, thereby identifying boundaries of landslide risk zones from a stable land area [7], [8].

However, topographical irregularities such as elevation, slope, and aspect to the radar line of sight (LOS) at the installation location [9] and temporal decorrelation of the interferometric data [10], especially due to atmospheric phase screen (APS), become challenging when large-scale observation areas are required. It creates an additional phase value that does not relate to the true displacement of the ground. These phase changes with topographical factors adversely affect the corresponding ground regions of the acquired SAR images, which do not correlate with true movement of the ground surface or estimated LOS displacement. This major limitation associated with the widespread GB-SAR deployment must be compensated to obtain reliable deformation information from unstable land areas, specifically for ground displacement monitoring in a mountainous environment [11], [12].

Spatio-temporal variation of APS is often modeled as a wavelength component in the unwrapped phase [13]. The tropospheric phase delay component due to APS is separated into two components, namely, the stratified APS delay and the stochastic (turbulent) APS delay. The stratified APS or hydrostatic delay correlates with the low-spatial frequency refraction index gradient [14]. This delay component is systematic and can be modeled [15]. On the contrary, the propagation speed of the electromagnetic signal fluctuates because of the temporal weather variations attributable to the mountain region topography, which is often referred to as the stochastic or turbulent APS [14]. Those two phenomena adversely affect the radar interferometric observations [16], creating the need for compensation.

Several phase compensation methods have been proposed [6]–[8]. One common approach, i.e., phase compensation by meteorological observation, is based on the estimation of the refractive index [17] during the GB-SAR monitoring period. The coherent-based algorithm [6] is a successive approach, where the phase disturbance is evaluated around the motionless pixels in the SAR image by active and passive control points. However, this method assumes the spatial homogeneity of the atmospheric refraction index between the sensor position and the illumination

Manuscript received May 31, 2019; revised October 18, 2019, December 12, 2019, January 29, 2020, and May 21, 2020; accepted June 18, 2020. Date of publication June 23, 2020; date of current version July 8, 2020. This work was supported in part by JSPS Grant-in-Aid for Scientific Research (A) under Grant 26249058 and in part by Tohoku University-NICT Joint Matching Project. *(Corresponding author: Amila Karunathilake.)*

Amila Karunathilake is with the Advanced Technologies Research Laboratory, Asia Air Survey Company, Ltd., Kawasaki 215-0004, Japan (e-mail: dr.amilatk@gmail.com).

Motoyuki Sato is with the Center for Northeast Asian Studies, Tohoku University, Sendai 980-8577, Japan (e-mail: motoyuki.sato.b3@tohoku.ac.jp).

Digital Object Identifier 10.1109/JSTARS.2020.3004341

area, which can only be justified for short ranges and small scenes.

Statistical analysis of the APS phenomena was proposed [8] based on the refinement of the tropospheric delay model using the humidity calibration. However, the analysis was conducted on a strong, stable target, and the longer-term acquisitions were compensated by an internal calibration scheme, both of which are impractical for a remote operation system. The coherence-based multiple-regression model technique [18] is one of the more reliable and practical approaches presented among the recent GB-SAR studies, which addresses the APS estimation as a homogenous atmosphere, and a second component that depends on height. However, the fluctuation of atmospheric temperature, pressure, and humidity has to be measured to obtain the absolute phase of the atmospheric artifacts and to examine the reliability of the method [19] for a specified study area, which is difficult on steep terrain with limited access and unfeasible for the real-time displacement data processing. In another approach, permanent scatters analysis [20] has been proposed, wherein prior knowledge of the area under the APS is needed from known motionless ground control points, which is rarely available during remote monitoring of construction sites with constant environmental changes caused by daily construction work.

Therefore, an atmospheric phase compensation method is proposed herein based on spatial modeling of the interferometric phase, especially for real-time GB-SAR monitoring. The rest of this article is organized as follows. In Section II, a general description of the observation area and the GB-SAR system and its configuration are discussed. The APS and its spatial inhomogeneity are then examined and the algorithm for the APS removal is proposed in Section III. The proposed algorithm was applied to APS compensation in a real-time GB-SAR monitoring station and the results are presented in Section IV. The obtained results and a comparative analysis of the estimated displacement were discussed to evaluate the reliability of the proposed method. Conclusions are finally presented in Section V.

II. Study Area Description and System Parameters

The studied area is located in Kyushu Island (South Japan), ranging from 50 km east of Kumamoto city to 3 km west of the Aso volcanic mountain. A large number of earthquake-triggered landslides had occurred around this area after the Kumamoto earthquake in 2016 [21], [22], with the largest reported landslide occurring in the western tip of the Aso caldera in the Minami-Aso area, as shown in Fig. 1. The elevation of this area varies from 9 m at the Kurokawa River to 1592 m at the Aso mountain peak, thereby contributing to the variation of atmospheric parameters. A GB-SAR system continuously operated over this area as an early warning system for the recovery workers who are involved with road reconstruction work from March to July 2017, and from March 2018 until the present day.

The GB-SAR system employed herein contains a radar sensor, power unit, and linear rail mounted on a one-meter high concrete base to stabilize the system on a plane horizontal to the ground. It facilitates the continuous movement of the radar unit by the mechanical system, as shown in Fig. 1. The technical parameters of the GB-SAR system are listed in Table I.

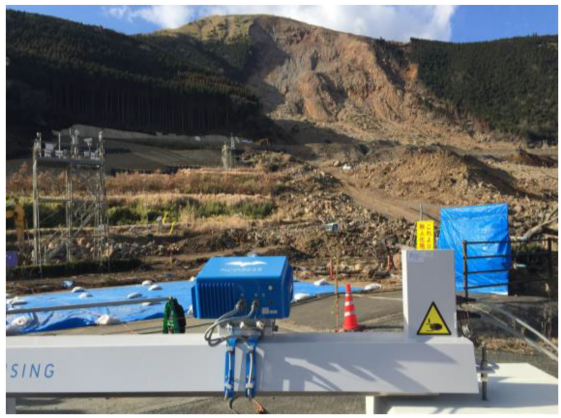

Fig. 1. Photo was taken after the landslide in the western tip of the caldera in Minami-Aso triggered by the catastrophic earthquake in Kumamoto prefecture on April 2016, including the GB-SAR system.

TABLE I
GB-SAR Parameters

System Parameters	Magnitude
Center frequency	17.2 GHz
Bandwidth	300 MHz
Rail length	1.8 m
Maximum range	1 km
Polarimetry	HH
View direction	315°
Tilt angle	15°
Data acquisition interval	15 min

The system works through an external ac power source that continuously charges two batteries, keeping the system steady and in operation during a power failure. The operating PC of the radar and rail unit is connected to a high-speed internet system to transfer the acquired GB-SAR data to the processing PC in Tohoku University, Miyagi Prefecture (Northeast Japan).

GB-SAR is accorded with the DInSAR technique for displacement estimation. One of the main advantages of differential interferometry is that the estimated differential phase $\Delta\varphi$ can be directly converted to the equivalent range displacement Δr, i.e., deformation in the LOS direction

$$\Delta\phi = \frac{4\pi}{\lambda}\Delta r \tag{1}$$

where λ refers to the wavelength of the transmitted signal. In advanced situations, the unambiguous displacement below $\lambda/2$ is accurately reconstructed without any phase-wrapping technique. A 2-D interferometric phase diagram covering 900 m in range distance and 500 m in cross-range distance by 2000×404 SAR pixels estimated by the Minami-Aso GB-SAR monitoring system are depicted in Fig. 2. Each of the image pixels represents the changes in the interferometric phase during the consecutive acquisition and displayed as a false-color image. The studied area can easily be distinguished from the surrounding noise in Fig. 2(a). The open soil layer shows an interferometric phase of zero, indicating no LOS displacement during the period. However, (1) assumes that the homogeneity of the transmission medium in the temporal domain is preserved, implying that the

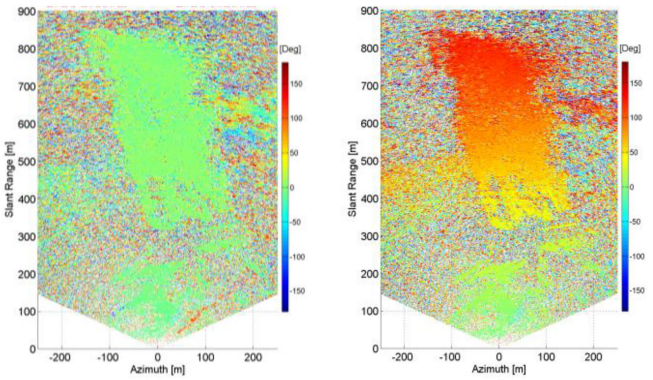

Fig. 2. 2-D interferograms received from GB-SAR with (a) no atmospheric effect and (b) with atmospheric effect along the range direction.

transmission medium remains the same in consecutive acquisitions and that Δr can be interpreted as the LOS physical displacement of the target. In practical applications, this assumption is invalid due to the presence of the APS, as depicted in Fig. 2(b).

III. Atmospheric Phase Screen

The electromagnetic signal transmitted by the GB-SAR propagates through the troposphere before reaching its destination. Due to the temporal change of atmospheric parameters, such as temperature, pressure, and relative humidity [6], the propagation velocity can be rapidly changed. This phenomenon is often seen in mountainous regions with frequently changing weather conditions. This can be minimized by selecting an optimum data acquisition interval for GB-SAR monitoring [10]. However, the temporal decorrelation of interferometric phases poses a significant problem for the GB-SAR monitoring site in the mountainous regions, as shown.

APS and its sudden changes affect the interferometric phase estimation process. The physical existence of the APS is based on the modulation of the electromagnetic wave's propagation velocity, which strictly depends on the change in the refractive index (Δn) of the troposphere caused by the fluctuation in meteorological parameters.

In general, this phase anomaly $\Delta\varphi_a$ can be estimated as follows [6]:

$$\Delta\phi_a = \frac{4\pi f_c r}{c}\Delta n \tag{2}$$

where f_c is the center frequency and c is the speed of light in vacuum. Thus, $\Delta\varphi_a$ is linear with respect to range r and phase anomaly is only caused by Δn. A series of interferometric phase diagrams affected by an APS and corresponding phase compensation diagrams after using a conventional method are shown in Fig. 3. The interferometric phase change along the range direction can easily be distinguished from the surrounding noise by its temporal stability, as depicted in Fig. 2(a). Different color scales were used to represent the observed phase anomaly within the 0° to 180° and 0° to −180° range to identify any phase wrapping. However, each interferogram in Fig. 3 neither exceeded this range nor demonstrated repeated circles during the specified interval of the data acquisition, indicating that no phase wrapping phenomena were observed within the maximum range distance of 900 m.

The phase changes caused by APS and phase anomaly are shown in Figs. 2(b) and 3(c), respectively, which can be identified as the two different scenarios of APS due to spatial distribution. The APS in Fig. 2(b) has a constant phase increment from the GB-SAR sensor to its maximum range of 900 m. The color scale shows that all image pixels in the interferogram lay from 0 to 180 in the positive phase region. This can be identified as an APS caused due to the changes in weather conditions or, in another word, the hydrostatic delay that can be compensated by evaluating the atmospheric influence on the interferometric phase [11], because the phase ramp has a constant gradient along the LOS direction. The phase gradient from the entire interferogram was removed and no residuals or phase anomalies were left by applying a conventional APS compensation method, as shown in Figs. 3(a) and 2(b) for non-APS and normal APS, respectively. However, the received interferogram, as shown in Fig. 3(c), shows a more severe effect of the APS. Herein, phase residuals remained after the application of a conventional APS removal method, as shown in Fig. 3(d). Therefore, the APS in Fig. 3(c) cannot be modeled with the conventional phase-compensation method since it did not demonstrate a constant phase increment from the GB-SAR sensor position to its maximum range of 900 m. Furthermore, (2) is only applicable for homogeneous atmospheres, i.e., when the pressure, temperature, and humidity change uniformly. As shown in Fig. 3(d), this assumption does not always stand due to the extremities in the mountainous weather conditions. Herein, an interferometric phase increment of 0°–100° is seen from approximately 0–400 m and phase decline began before the phase boundary of 180° at the next slope's surface. Thus, the conventional APS model could not be applied as a general solution for all the received interferograms. The limitation for application in all weather conditions must be overcome by an algorithm that is capable of handling normal and extreme weather conditions for real-time data processing. Therefore, a more adaptive approach must be considered for APS removal.

Environmental monitoring by GB-SAR systems varies with changing geomorphology, especially in mountainous regions. An accurate estimation of the spatial dissemination of a radiated signal [9] would assist in obtaining the inestimable information about the monitored land prior to hardware deployment. Therefore, a 3-D model, depicting the western tip of the Aso caldera in Fig. 4, was developed to examine the dependence between the GB-SAR illumination area and the geomorphology of the terrain. Herein, the triangular-shaped post-landslide site faced the east and is divided by the line AC. The terrain lines on the left and right sides, i.e., sides D and E, respectively, represent the remaining natural land surface, whereas the line along AC represents the land area affected by slope failure after the earthquake.

A 3-D simulation of expected ground illumination by GB-SAR was evaluated using the digital elevation model generated by LiDAR [10] and is shown as a terrain model in Fig. 5. The

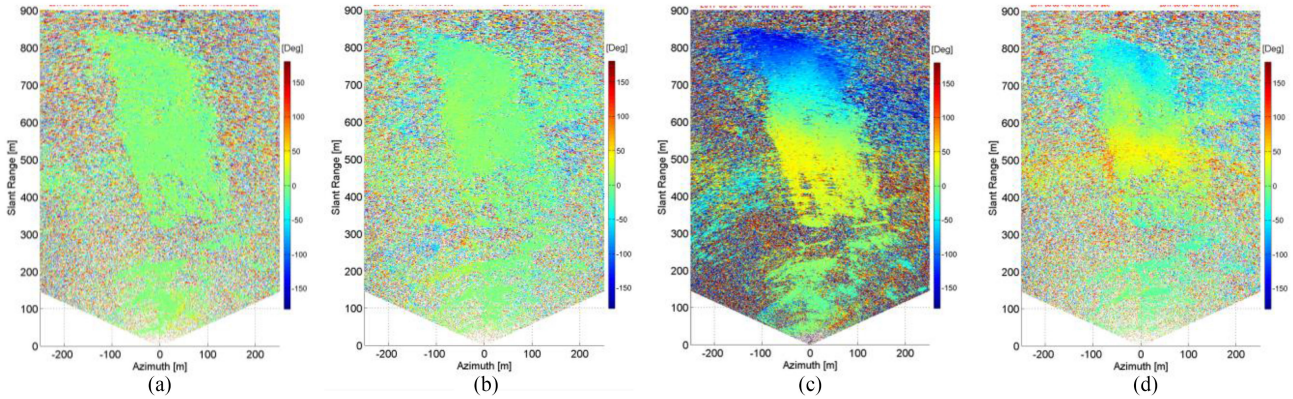

Fig. 3. Randomly selected 2-D interferograms (a) after applying a conventional method for no APS, (b) after applying a conventional method for normal APS, (c) severely affected by APS due to extreme weather conditions, and (d) after applying a conventional APS removal method to the severely affected interferograms in extreme weather conditions.

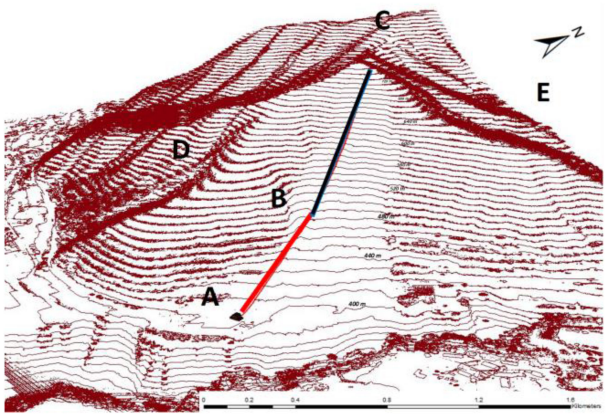

Fig. 4. 3-D terrain model of the Minami-Aso area, where point A represents the installation location of GB-SAR facing to the mountain peak (in point C). Points D, B, and E are at the same altitude.

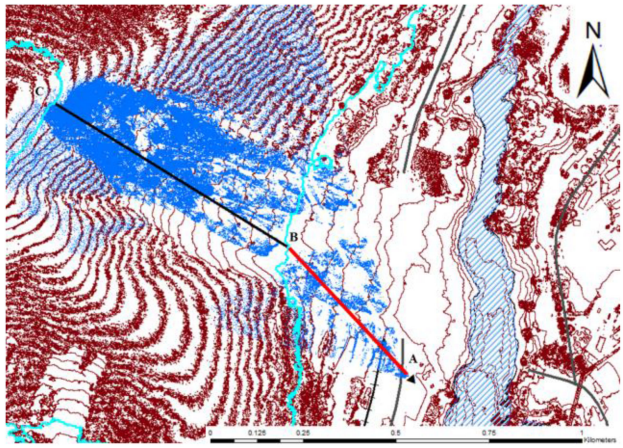

Fig. 5. Terrain model of the monitoring area with the estimated illumination of the GB-SAR shown in dark blue overlay.

GB-SAR was operated from location A facing the mountain peak C to illuminate the 0.45 km^2 area around the line AC that was affected by landslides. The estimated illumination results were projected onto a 3-D model to provide the aerial view of the scene shown in Fig. 5. Herein, radar would provide higher illumination to the steep terrain in BC than the moderate slope surface in AB. Points D, B, and E were all at an elevation of 400 m, and can, thereby, be used to represent a boundary between the different slope surfaces AB and BC. The altitude and range distances were computed using a cross section of the 3-D model in the radar's LOS plane, as shown in Fig. 6. During the system calibration time, preliminary DInSAR images depicted a diverse behavior for the phase change in slope surface AB and BC.

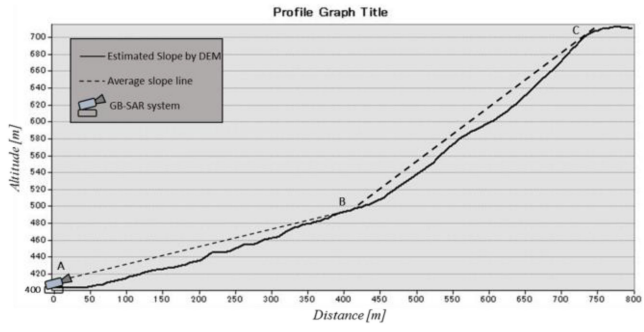

Fig. 6. Cross section of the mountain in radar LOS plane.

A. Coherence Scatter Selection

Coherence scatter (CS) selection is necessary for displacement monitoring in far-range applications to understand the overall phase change of the DInSAR image. Many proposed APS correction methods rely on the CS response [6]–[8]. If the CSs are predefined by the installation of the stable reflectors, atmospheric correction can be performed by correcting the response of their CS phase. However, in this steep terrain, the CSs are unknown; therefore, they must be selected from acquired SAR images of the observed area. Conventionally, the CSs are selected by estimating the dispersion index $D_{m,n}$ that quantifies the variation in amplitude through a number of images taken

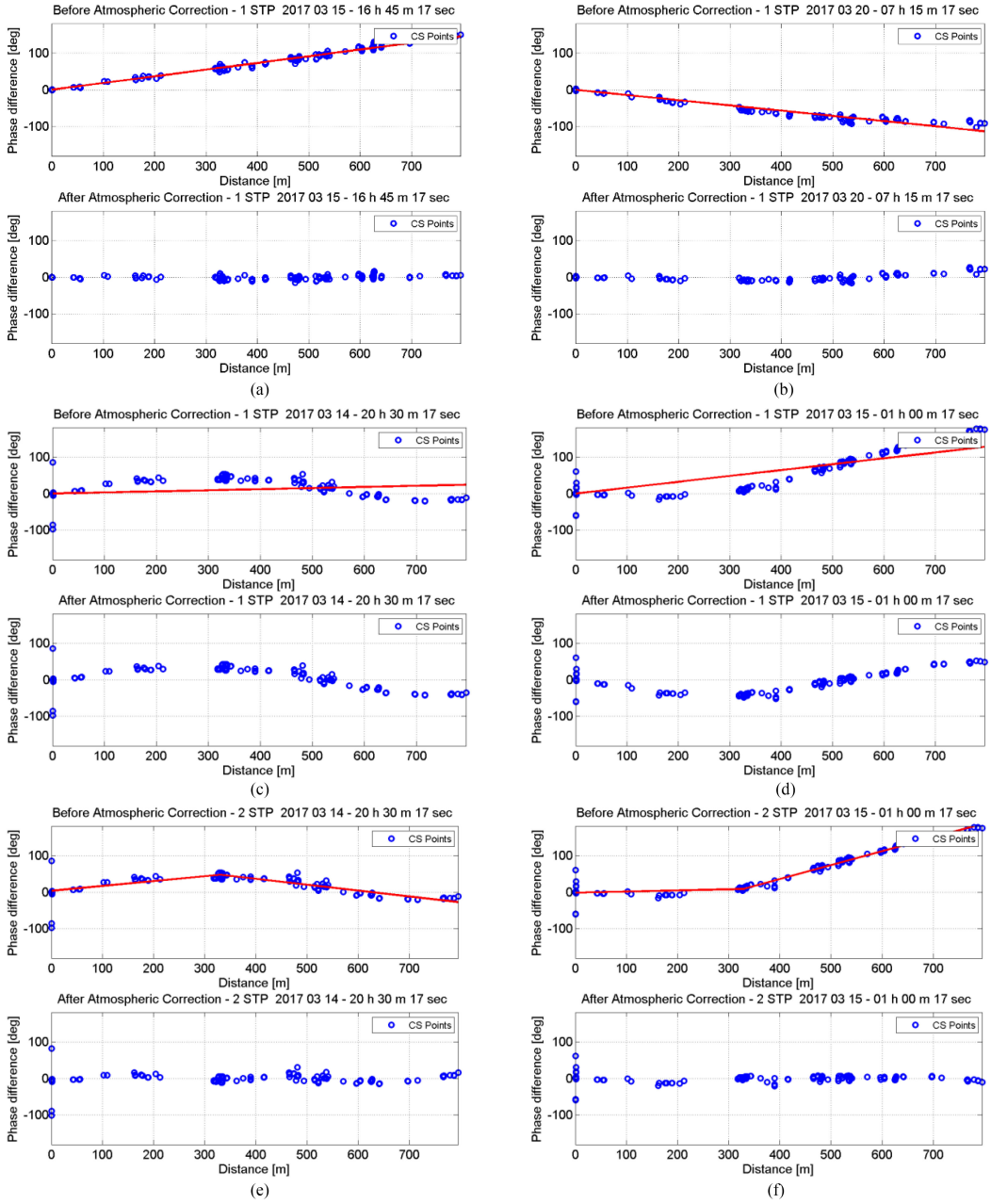

Fig. 7. Representation of CS phase changes due to atmospheric artifact: observed phase changes of CS points in normal weather at (a) time t_1 and at (b) time t_2, before and after applying for APS compensation. Observed phase changes of CS points in extreme weather conditions at (c) time t_3 and at (d) time t_4, before and after applying the conventional APS compensation method. Observed phase changes of CS points in same weather conditions at (e) time t_3, and (f) time t_4, before and after applying the proposed method for APS compensation.

over different time lapses and obtained as [23]

$$D_{m,n} = \frac{\sigma_{m,n}}{A_{m,n}} \tag{3}$$

where m and n refer to the pixel row and column, respectively. $A_{m,n}$ is the mean amplitude with respect to the time lapse, and $\sigma_{m,n}$ is the standard deviation of the amplitude. The landslide caused the studied terrain to be heavily altered at and surrounding the newly exposed mountain cliff. Both the eroded surface and deposited layer produced a constant reflection with a lower dispersion over time than the surrounding tree canopy. The higher mean amplitude favors lower dispersion in the CS values. Therefore, CSs with lower dispersion indexes were distributed in this eroded area, which has the highest priority for displacement estimations. Those points were located along the range direction and their range positions are shown in the range phase diagrams in Fig. 7.

B. *Failure of Conventional APS Compensation Method*

Conventional atmospheric phase removal uses a linear phase ramp estimated through a simple linear regression model over

the range axis [24]–[27], providing a smaller phase difference in the near range and larger phase difference in the far range. Herein, each CS phase corresponding to the selected CS points in the range direction was used to understand the APS by its spatial distribution over time. Fig. 7(a) and (b) shows the interferometric phase of the same CS points over two different times. The calculated phase residual was used to estimate the regression in each of the interferograms, as shown with red lines, where nearly all CS points had a low-standard error and were on the estimated line. The conventional regression line can be used as an APS estimator to compensate for the phase ramp in normal weather conditions.

However, the phase changes of the same CS points over a different time t_3 and t_4 are shown in Fig. 7(c) and (d), respectively. Herein, the conventional linear regression model had a larger standard error and used phase residuals, which caused an erroneous estimation of phase compensation. Therefore, the estimated linear regression from the conventional method is inadequate for reliable measurements. Consequently, the interferometric phases of the near- and far-range CS points in Fig. 7(c) were overestimated and underestimated, respectively. This was interchanged in consecutive interferograms in Fig. 7(d). Therefore, the phase compensation method could not be applied if the phase delay is not linear with the range in mountainous areas.

C. Spatial Inhomogeneity of Reflected Phase

Steep topographical variation often causes extreme weather conditions, resulting in random and rapid fluctuation of atmospheric parameters, such as temperature, pressure, and humidity, as demonstrated by the interferometric phase data received from the Minami-Aso GB-SAR monitoring site originally shown in Fig. 4. Randomly selected datasets of the CS phase, as shown in Fig. 7(c) and (d), prove that the sudden change of the phase ramp between the lower and upper stages breaks the homogeneity of the conventional refraction model [7]. It fails in situations with large variations in terrain topography, i.e., also more challenging to existing theoretical techniques, when compared with an empirical model. The backscatter radar signal of the GB-SAR simulation results can be divided into two stages according to the surface illumination, i.e., near the radar, indicated by area AB and far from the radar, indicated by area BC. In stage 1, the AB distance had a high-incidence angle due to the average slope gradient of the observation terrain. In stage 2, represented by the BC line, the higher surface slope gradient (lower incidence angle) and LOS orientation led to greater backscattering. This compromised the conventional APS model, which relies on the spatial homogeneity of the refraction index. Due to the spatial inhomogeneity of the reflected surface, the observed CS phase change depicted a diverse change in both the near- and far-field range. The data could be separated into two basic sections by considering the interferometric phase fluctuation and the range distance of the CS points located on the surface of each slope. As shown in Fig. 7, the observed changes in the CS phase frequently varied with time t_1, t_2 and t_3, t_4, due to the extreme weather conditions near the mountain and had an implicit correlation with the spatial model due to the elevation profile of the observation area. However, changes in the CS phase become random with time, depending on the weather condition in each slope surface of the total monitoring range. Therefore, a more precise model correlated with geographical information, such as an atmospheric artifact removal model with spatial terrain information, is required for more reliable displacement estimation.

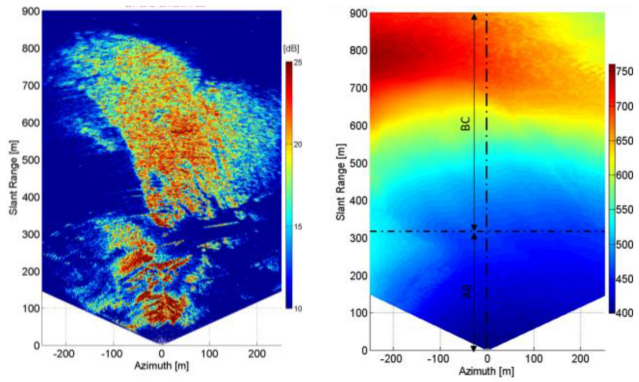

Fig. 8. (a) Amplitude image of reflected GB-SAR signal (b) Cross section of elevation versus ground range in two different slope surface by radar coordinate system.

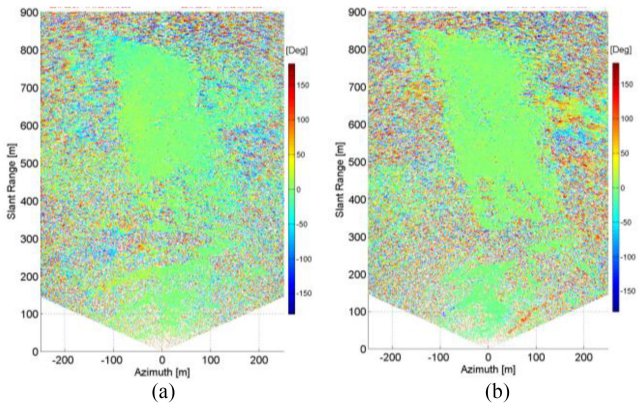

Fig. 9. After applying the proposed TSSA into the 2-D interferograms (a) normal weather conditions and (b) extreme weather conditions.

D. Two-Stage Semiempirical Algorithm

According to the elevation information of the 3-D model and observed interferograms, the estimated CS phases indicate errors for the conventional GB-SAR displacement monitoring system, including abnormal phase incrementing at two specific stages in the range direction due to the random changes of atmospheric parameters in the mountainous weather condition. In Fig. 8(a), the 2-D amplitude image of the GB-SAR signal depicts spatial dispersion of the reflected signal in two stages of the slope surfaces. The elevation versus ground range [see Fig. 8(b)] simplifies the 3-D DEM information into a 2-D radar coordinate to identify the margins of each stage in the following equation. Therefore, a two-stage model can be used to correct the total phase change, using two separate linear models that

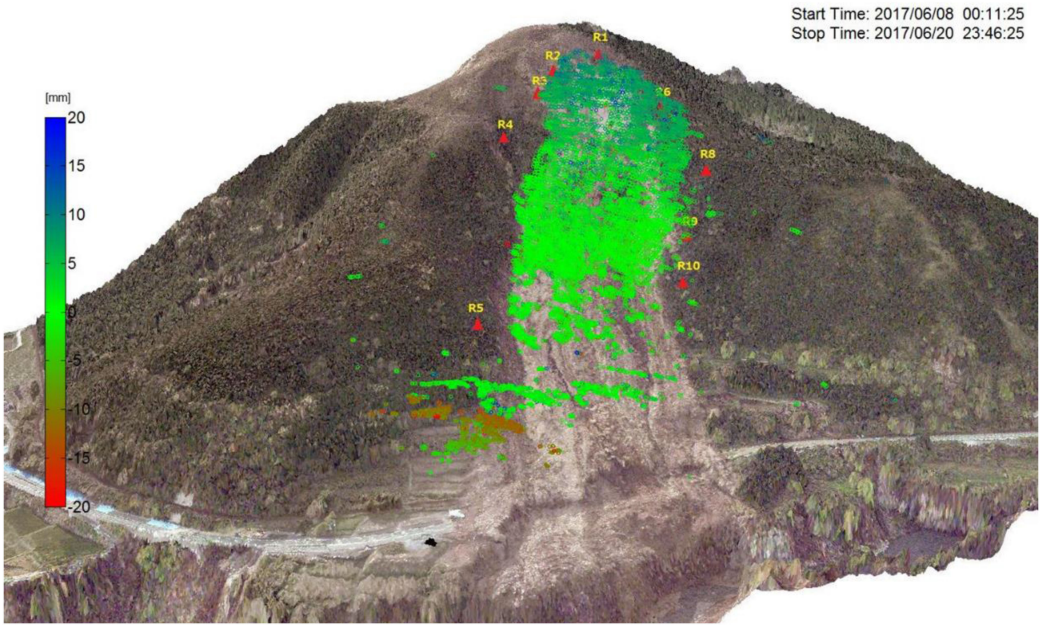

Fig. 10. Estimated displacement of the CS points acquired by GB-SAR montioring in postlandslide site in Minami-Aso, Kumamoto.

represent the temporal phase change of the CS points over the range of AB and BC. A two-stage model was, thus, proposed to estimate the slant range distance in each elevation plane using a spatial model

$$\Delta\varphi_{i^{\text{th}}\text{corr}} = \arg\left\{\exp\left[j\int_1^w(\Delta\phi_i - y_1)dr\right] + \exp\left[j\int_w^n(\Delta\phi_i - y_2)dr\right]\right\} \quad (4)$$

where $\Delta\varphi$ is the measured interferometric phase, which was affected due to the atmospheric change, and y_1 and y_2 are the estimated functions for APS removal in each elevation layer, bounded by w in the slant range r direction, as

$$y_1 = a_1 r + c_1, \quad r < w \quad (5)$$

$$y_2 = a_2 r + c_2, \quad r \geq w. \quad (6)$$

The liner functions y_1 and y_2 correspond to the LOS range are depicted in Fig. 6 from A to B and B to C in the empirical model. The constants a_1, a_2, c_1, and c_2 were estimated [26] in each pixel along the range direction of acquired interferograms by the piecewise linear regression model

$$y_i = \sum_{k=0}^{N} a_k r_{ki} + c_i \quad (7)$$

where a_k is the regression coefficient and c_i is the coefficient for the intercept in the linear regression model. Due to the temporal change of the APS, the phase gradient was estimated for each stage in the range direction, as shown in Fig. 7(e) and (f). Here, the first and second stages have a different phase gradient that changes according to the observed CS phase in the near- and far-range regions. Unlike near range observations, GB-SAR monitoring in the far range shows limitations, but by considering the quality of the received signal, the robustness of the displacement information is obtained. The estimated phase gradient and APS affected CS phase show a significant reduction in the phase variance associated with the pooling effect of the piecewise linear regression model. In theory, adding more than two regimes to the piecewise linear functional (for a large variation in the terrain topography) increases the accuracy of APS estimation and the robustness of the estimated displacement. However, in practice, this introduces an inconsistency between the estimated displacement and the real movement of the slope surface. To preserve the reliability of displacement measurements and limitations of GB-SAR in far-fielded observations during extremes in the weather condition, the two-stage semiempirical algorithm (TSSA) shows the best performance in APS estimation and reduction among the methods tested in this study. Moreover, under normal weather conditions, phase anomaly can be estimated by the linear regression model. Hence, the a_1, a_2, c_1, and c_2 regression coefficients coincide, yielding a linear model with a single gradient as in the conventional APS removal method. Therefore, the proposed model can be used for remote monitoring under normal and extreme weather conditions alike.

IV. Results and Discussion

The proposed model was implemented at the Minami-Aso landslide early warning site and the APS was evaluated at both the elevation stages. The results in Fig. 7 shows the range vs. the phase diagram of the CS locations by conventional and proposed

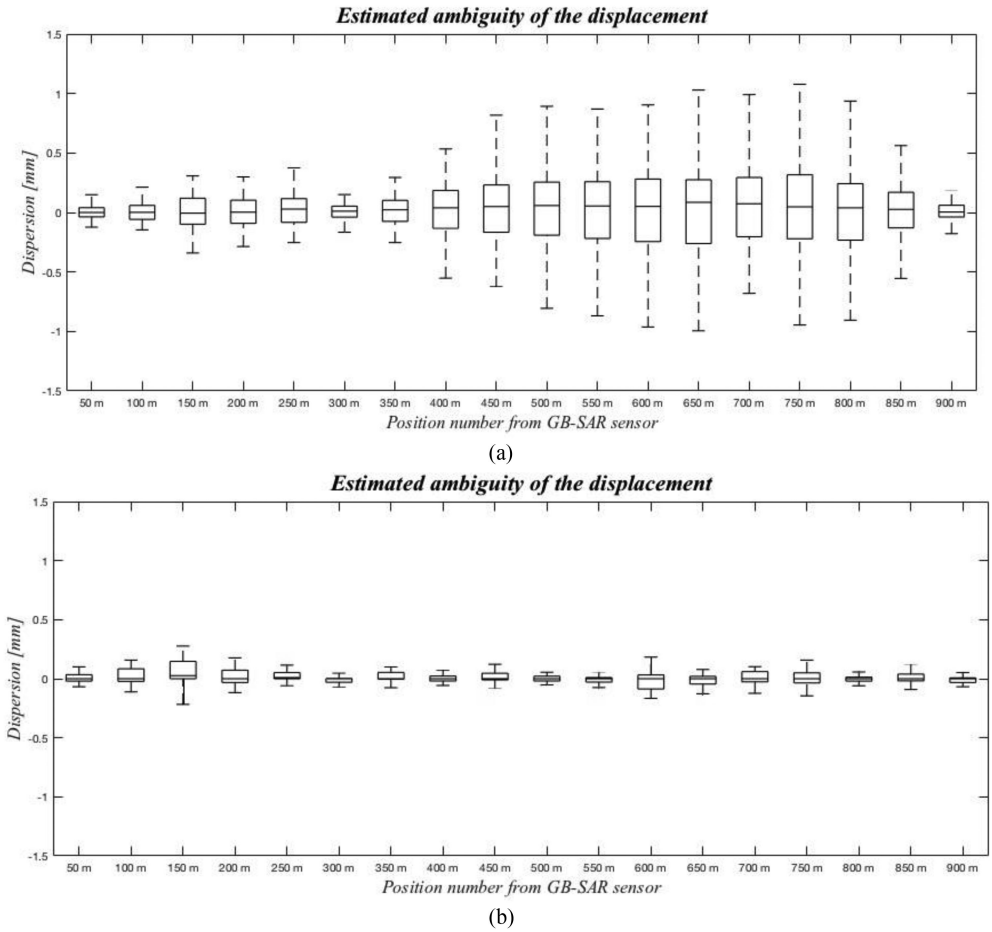

Fig. 11. Mean-phase ambiguity of APS estimation results in (a) conventional APS removal method and (b) TSSA in Minami-Aso GB-SAR monitoring site.

APS removal methods. The proposed method estimates the APS for each interferogram, with an estimated phase error of each slope compensated by the piecewise linear regression model. The calculated phase gradient of each model varies due to extremes in the weather condition. Thus, each interferogram undergoes phase estimation and corresponding compensation with time. Therefore, the proposed TSSA is a dynamic model that produces zero-phase difference in the observation area after atmospheric phase compensation for the 2-D interferogram in extreme weather conditions. Unlike conventional models, the proposed method preserved the phase continuity by giving the lowest phase residual. The applicability of the proposed APS estimation is shown in Fig. 7(e) and (f) for the two different interferometric datasets at different time intervals. During the GB-SAR monitoring period, the mean displacement of the ground area along the radar LOS direction was considered. Critical displacement was not reported from the construction site; however, the high ambiguity of the displacement was observed with the conventional method due to its inapplicability.

The proposed algorithm provided a lower phase residual than the conventional APS removal methods. The resulting 2-D interferograms after applying the proposed TSSA in normal and extreme APS are depicted in Fig. 9; in both, the APS has been compensated for with minimum phase residual. Due to the inhomogeneity and temporal fluctuation of the atmospheric parameters, the interferometric phase shifts along with the radar LOS and its sudden fluctuation adversely affected the estimated displacement. In the proposed method, the estimated atmospheric phase error was compensated for in normal and extreme weather conditions. Therefore, the proposed method provided an optimal phase screen removal during GB-SAR monitoring in a mountainous region. Conventional methods that are used to remove the APS are based on randomly located targets, which are less sensitive for natural terrain, leading to under or overestimation of the CS in the near and far ranges, respectively, and large errors in displacement estimations. In the proposed method, the APS estimation was identical for the particular slope surface. Therefore, APS-caused phase changes along the slope surfaces were calculated, allowing for displacement results that were sensitive to the actual displacement of the slope's surface. The proposed regression approach is less sensitive to high spatial-frequency fluctuation in refractivity utilizing the pooled estimation forced by the piecewise regression. The estimated cumulative displacement of the post-landslide area during the observation period is shown and projected into a 3-D model in Fig. 10.

The majority of the CS points in green color represent the zero displacements over the monitoring period. The blue and red

colors represent the CS point movement toward and away from the radar, respectively. During the first quarter of the year, critical slope failures were not recorded. However, due to the number of recorded earthquakes during the road reconstruction period, recent and updated stability information was necessary to plan the daily construction work. Therefore, real-time atmospheric phase compensation results were necessary to provide a reliable estimation of the displacement location during the monitoring period. This information is continuously displayed in a 3-D model (see Fig. 10) refreshed every 15 min all day (24 h), providing remote access to institutions responsible for road reconstruction.

The data in Fig. 7(c) and (d), at times t_3 and t_4, illustrate the phase gradient estimated from alternative directions in each slope, highlighting its variation with time. Therefore, the data in Fig. 7 clarify that neither the elevation-dependent term nor the constant slope gradient is unusable for APS estimation due to the alternation of the APS. To facilitate a fair performance comparison of the proposed method, we examine the validity of the proposed method compared with the conventional APS method. A comparison of the estimated mean values of the phase residual using the conventional and proposed TSSA is depicted in Fig. 11. In the conventional method [see Fig. 11(a)], there is a larger mean-phase dispersion in the far range than in the near range, indicating the ambiguity of the conventional APS removal method for slope surface monitoring. The observed phase fluctuation varied in a higher range of values as depicted by the maxima and minima (whiskers) of each boxplot evaluated in every 50 m range distance. However, the proposed model has a minimum value for the whiskers in the same validation time. The mean value of the maxima and minima of each box and whisker plot shown in Fig. 11(b) had a lower dispersion for the same dataset, indicating that the proposed method improved the APS estimation and minimized phase dispersion in both the near and far range. During this period, no critical slope failures were recorded. Some soil accumulation was noticed between 600 and 750 m due to some construction work in the top-left corner of the mountain. This statistical validation, thus, indicates that the proposed method was superior for GB-SAR monitoring in mountainous regions with extreme weather conditions.

Furthermore, the data processing method of the proposed TSSA does not require background information, such as meteorological parameters with postprocessing steps. Therefore, TSSA optimally estimates differential phases in real-time for the entire interferogram by eliminating the APS disturbances, providing an increase in both efficiency and reliability of the total GB-SAR monitoring process. Thus, reliable estimations of the ground displacement can be performed over the monitoring area to provide early warnings of landslides to the people working at the base of the mountain.

V. Conclusion

A DInSAR technique of GB-SAR was used to identify the displacement of steep terrain at a disaster recovery site in Minami-Aso, Kumamoto. Interferometric phase changes caused by the varying weather conditions were observed. Due to the complicated geomorphology of the area and resulting temporal variation in atmospheric parameters, conventional methods to measure the displacement in time and space domains often provide highly inaccurate results. A 3-D spatial model was used to examine the spatial inhomogeneity of the interferometric phases. The phase changes of two elevation layers showing varying phase gradients with atmospheric conditions were examined along with the radar LOS. A dynamic TSSA model that estimates the phase gradient of each layer based on piecewise linear regression modeling was, therefore, proposed to remove this phase change in the spatial domain. The proposed method is based on a spatial model and statistical compensation methodology compensated for the spatial inhomogeneity without using temporal changes of atmospheric parameters, such as temperature, pressure, or humidity, allowing for accurate displacement measurements and the removal of the APS effect for GB-SAR measurements with less background information. Unlike conventional GB-SAR data processing, the proposed method does not require any implementation in collecting and processing meteorological data at a station and at any stage of an experiment. Therefore, the proposed method enhances the applicability of the GB-SAR, allowing it to be deployed as a fully remote, standalone system.

References

[1] K. Thuro *et al.*, "New landslide monitoring techniques—Developments and experiences of the alpEWAS project," *J. Appl. Geodesy*, vol. 4, pp. 69–90, 2010.

[2] S. Uhlemann *et al.*, "Assessment of ground-based monitoring techniques applied to landslide investigations," *Geomorphology*, vol. 253, pp. 438–451, 2016.

[3] S. Placidi, A. Meta, L. Testa, and S. Rodelsperger, "Monitoring structures with FastGBSAR," in *Proc. IEEE Radar Conf.*, Johannesburg, South Africa, 2015, pp. 435–439.

[4] K. Takahashi, M. Matsumoto, and M. Sato, "Continuous observation of natural-disaster-affected area using ground-based SAR interferometry," *IEEE J. Sel. Topics Appl. Earth Observ. Remote Sens.*, vol. 6, no. 3, pp. 1286–1294, Jun. 2013.

[5] F. T. Ulaby *et al.*, *Microwave Radar and Radiometric Remote Sensing*. Ann Arbor, MI, USA: Univ. Michigan Press, 2014.

[6] L. Pipa, X. Fabregas, A. Aguasca, and C. Lopez-Martinez, "Atmospheric artifact compensation in ground-based DInSAR applications," *IEEE Geosci. Remote Sens. Lett.*, vol. 5, no. 1, pp. 88–92, Jan. 2008.

[7] K. Takahashi, M. Matsumoto, and M. Sato, "Coherent scatterer selection based on coherence of interleaved sub-image for atmospheric correction of ground-based synthetic aperture radar interfermoetry," in *Proc. IEEE Int. Geosci. Remote Sens. Symp.*, Melbourne, VIC, Australia, 2013, pp. 3891–3894.

[8] L. Iannini and A. M. Guarnieri, "Atmospheric phase screen in ground-based radar: Statistics and compensation," *IEEE Geosci. Remote Sens. Lett.*, vol. 8, no. 3, pp. 537–541, May 2011.

[9] A. Karunathilake and M. Sato, "3-D Model assisted survey to design and estimate ground based SAR illumination," in *Proc. 42nd Remote Sens. Symp., Soc. Instrum. Control Eng.*, Chiba, Japan, Mar. 2017, pp. 35–38.

[10] A. Karunathilake, L. Zou, K. Kikuta, M. Nishimoto, and M. Sato, "Implementation and configuration of GB-SAR for landslide monitoring: Case study in Minami-Aso, Kumamoto," *Exploration Geophys.*, vol. 50, no. 2, pp. 210–220, 2019.

[11] K. Senro, N. Yuichi, D. Ryosuke, and M. Kazutaka, "Monitoring ground deformation of eruption center by ground-based interferometric synthetic aperture radar (GB-InSAR): A case study during the 2015 phreatic eruption of Hakone volcano," *Earth, Planets Space*," vol. 70, no. 3, Nov. 2018, Art. no. 181.

[12] K. Tamura and A. Maeda, "Monitoring of lava dome of Unzen volcano by EDM and ground based synthetic aperture radar," *J. Jpn. Soc. Erosion Control Eng.*, vol. 65, no. 1, pp. 69–72, 2012.
[13] F. Onn and H. A. Zebker, "Correction for interferometric synthetic aperture radar atmospheric phase artifacts using time series of zenith wet delay observations from a GPS network," *J. Geophys. Res.*, vol. 111, no. B9, pp. 1–16, Sep. 2006.
[14] P. S. Agram and M. Simons, "A noise model for InSAR time series," *J. Geophys. Res. Solid Earth*, vol. 120, pp. 2752–2771, Apr. 2015.
[15] R. Jolivet *et al.*, "Improving InSAR geodesy using global atmospheric," *J. Geophys. Res. Solid Earth*, vol. 119, pp. 2324–2341, Mar. 2014.
[16] S. Baffelli, O. Frey, and I. Hajnsek, "Geostatistical analysis and mitigation of atmosphere induced phase in terrestrial radar interferometric observations of an alpine glacier," in *Proc. 12th Eur. Conf. Synthetic Aperture Radar Electron. Proc.*, Aachen, Germany, 2018, pp. 626–631.
[17] G. D. Thayer, B. R. Bean, and B. A. Hart, "Worldwide characteristics of refractive index and climatological effects," Environ. Sci. Services Admin., Boulder, CO, USA, Aug. 1970.
[18] R. Iglesias *et al.*, "Atmospheric phase screen compensation in ground-based SAR with a multiple-regression model over mountainous region," *IEEE Trans. Geosci. Remote Sens.*, vol. 52, no. 5, pp. 2436–2449, May 2014.
[19] R. Iglesias *et al.*, "Ground-based polarimetric SAR interferometry for the monitoring of terrain displacement phenomena—Part I: Theoretical description," *IEEE J. Sel. Topics Appl. Earth Observ. Remote Sens.*, vol. 8, no. 3, pp. 980–993, Mar. 2015.
[20] L. Noferini *et al.*, "Permanent scatterers analysis for atmospheric correction in ground-based SAR interferometry," *IEEE Trans. Geosci. Remote Sens.*, vol. 43, no. 7, pp. 1459–1471, Jul. 2005.
[21] K. Dang *et al.*, "Mechanism of two rapid and long-runout landslides in the 16 April 2016 Kumamoto earthquake using a ring-shear apparatus and computer simulation (LS-RAPID)," *Landslides*, vol. 13, pp. 1525–1534, Aug. 2016.
[22] Y. Yagi, R. Okuwaki, B. Enescu, A. Kasahara, A. Miyakawa, and M. Otsubo, "Rupture process of the 2016 Kumamoto earthquake in relation to the thermal structure around Aso volcano," *Earth, Planet Space*, vol. 68, Jul. 2016, Art. no. 118.
[23] A. Ferretti, C. Prati, and F. Rocca, "Permanent scatterers in SAR interferometry," *IEEE Trans. Geosci. Remote Sens.*, vol. 39, no. 1, pp. 8–20, Jan. 2001.
[24] G. Luzi *et al.*, "Ground-based radar interferometry for landslides monitoring: Atmospheric and instrumental decorrelation source on experimental data," *IEEE Trans. Geosci. Remote Sens.*, vol. 42, no. 11, pp. 2454–2466, Nov. 2004.
[25] R. F. Hanssen, *Radar Interferometry: Data Interpretation and Error Analysis*. Dordrecht, The Netherlands: Kluwer, 2001.
[26] M. S. Seymour and I. G. Cumming, "Maximum likehood estimation for SAR interferometry," in *Proc. IGARSS-Surface Atmospheric Remote Sens. Tec.*, Aug. 1994, pp. 2272–2275.
[27] E. K. Smith and S. Weintraub, "The constant in the equation for atmospheric reflective index at Radio frequency," *Proc. IRE*, vol. 41, no. 8, pp. 1035–1037, Aug. 1953.

Amila Karunathilake (Member, IEEE) received the Ph.D. degree in environmental studies from Tohoku University, Sendai, Japan, in 2017.

He was with The Advanced Technologies Research Laboratory, Asia Air Survey Company, Ltd., Kawasaki, Japan, and is currently working on disaster prevention research project under the Cross-Ministerial Strategic Innovation Promotion Program. He was a Postdoctoral Researcher with Tohoku University in 2018. His research interests include radar interferometry, ground-based synthetic aperture radar (GB-SAR), differential interferometric SAR, polarimetric SAR and 3-D spatial modeling, and LiDAR point cloud.

Dr. Karunathilake was a recipient of the Young Researcher Award from IEEE GRSS Japan Chapter and the best Ph.D. Student Award from the Graduate School of Environmental Studies, Tohoku University, in 2017.

Motoyuki Sato (Fellow, IEEE) received the B.E. and M.E. degrees and the Dr. Eng. degree in information engineering from the Tohoku University, Sendai, Japan, in 1980, 1982 and 1985, respectively.

Since 1997, he has been a Professor with Tohoku University. He was the Distinguished Professor of Tohoku University from 2007 to 2011 and the Director of the Center for Northeast Asian Studies, Tohoku University from 2009 to 2013. He was a Visiting Professor with Jilin University, China, Delft University of Technology, The Netherlands, and Mongolian University of Science and Technology. He was also a Visiting Researcher with the Federal German Institute for Geoscience and Natural Resources (BGR), Hannover, Germany, during 1988–1989. He developed GPR sensors for humanitarian demining, and they are used in mine-affected countries including Cambodia. His current research interests include transient electromagnetics and antennas, radar polarimetry, ground penetrating radar (GPR), borehole radar, electromagnetic induction sensing, GB-SAR, and MIMO radar systems.

Dr. Sato was the recipient of 2014 Frank Frischknecht Leadership Award from SEG for his contribution to his sustained and important contributions to near-surface geophysics in the field of ground-penetrating radar. He was also the recipient of the IEICE Best Paper Award (Kiyasu Award) in 2017, the Achievement Award in 2019, the IEEE GRSS Education Award in 2012, and IEEE Ulrich L. Rohde Innovative Conference Paper Awards on Antenna Measurements and Applications in 2017. He was a member of the IEEE GRSS AdCom from 2006 to 2014. He is also a Chair of IEEE Sendai section during 2020–2021. He is an Associate Editor for IEEE GEOSCIENCE AND REMOTE SENSING LETTERS, and a Guest Editor of the special issue of GPR2006 and GPR2010 in *Transactions on Geoscience and Remote Sensing*, and IGARSS2011, GPR2012 and GPR2014 in IEEE JOURNAL OF SELECTED TOPICS IN APPLIED ERATH OBSERVATIONS AND REMOTE SENSING. He was the Chair of the IEEE GRSS Japan Chapter during 2006–2007. He was the General Chair of IGARSS2011 and the Technical Chair of GPR1996.